

The enhancement of neutron-rich particle emission from out-of-fission-plane in Fermi energy heavy ion reactions

Yi-Jie Wang¹® · Sheng Xiao¹ · Meng-Ting Wan²,³ · Xin-Yue Diao¹® · Yu-Hao Qin¹® · Zhi Qin¹® · Dong Guo¹ · Da-Wei Si¹ · Bo-Yuan Zhang¹ · Bai-Ting Tian¹ · Jun-Huai Xu¹ · Fen-Hai Guan¹® · Qiang-Hua Wu¹ · Xiang-Lun Wei⁴ · He-Run Yang⁴ · Peng Ma⁴ · Rong-Jiang Hu⁴ · Li-Min Duan⁴® · Fang-Fang Duan⁴ · Jun-Bing Ma⁴ · Shi-Wei Xu⁴ · Qiang Hu⁴ · Zhen Bai⁴ · Yan-Yun Yang⁴® · Jian-Song Wang⁴,⁵® · Wen-Bo Liu⁶ · Wan-Qing Su⁶® · Xiao-Bao Wei⁶® · Chun-Wang Ma⁶® · Xin-Xiang Li²,⁵ · Hong-Wei Wang⁵,⁵® · Ying-Xun Zhang¹0® · Michał Warda¹³ · Arthur Dobrowolski¹³ · Bożena Nerlo-Pomorska¹³ · Krzysztof Pomorski¹¹ · Li Ou²,³® · Zhi-Gang Xiao¹,¹²®

Received: 6 January 2025 / Revised: 23 March 2025 / Accepted: 24 March 2025 / Published online: 9 June 2025 © The Author(s), under exclusive licence to China Science Publishing & Media Ltd. (Science Press), Shanghai Institute of Applied Physics, the Chinese Academy of Sciences, Chinese Nuclear Society 2025

Abstract

The neutron richness of the light charged particles emitted out of the fission plane in heavy ion reactions has been experimentally investigated via the production of A = 3 mirror nuclei in 86 Kr + nat Pb reactions at 25 MeV/u. The energy spectra and angular distributions of triton (t) and 3 He in coincidence with two fission fragments are measured with the Compact Spectrometer for Heavy IoN Experiment (CSHINE). The energy spectrum of 3 He is observed harder than that of triton in the fission events, in accordance with the phenomena reported as " 3 He-puzzle" in inclusive measurements. With a data-driven energy spectrum peak cut scenario, it is observed that the yield ratio $R(t/^{3}$ He) increases with the angle to the fission plane, showing an enhancement of neutron-rich particle emission from out-of-fission-plane. A qualitative comparison with the transport model calculations suggests that this observation may serve as a new probe for the nuclear symmetry energy.

Keywords Heavy ion reaction \cdot Fast fission \cdot ³He-puzzle \cdot Out-of-fission-plane emission \cdot Nuclear symmetry energy

1 Introduction

Heavy ion reactions (HIR) provide a femtoscopic laboratory for investigating the properties of the nuclear equation of state (nEoS), particularly the nuclear symmetry energy $E_{\rm sym}(\rho)$ [1–6]. The stringent constraint of $E_{\rm sym}(\rho)$ is crucial for both nuclear- and astrophysics and draws the most attention since the detection of the gravitational waves from the neutron star merging event GW170817 [7–9]. Although great progress has been made via neutron skin thicknesses[10–14], nuclear charge radius[15], flow[16–18] and

This work was supported by the National Natural Science Foundation of China (Nos. 12205160, 11961131010, 11961141004, and 11965004), and by the Ministry of Science and Technology of China (Nos. 2022YFE0103400 and 2020YFE0202001), and by the Polish National Science Center (No. 2023/49/B/ST2/01294). This work is also supported by Initiative Scientific Research Program and the Center of High Performance Computing of Tsinghua University, and the Heavy Ion Research Facility at Lanzhou (HIRFL).

Extended author information available on the last page of the article

the detection of isobaric yield ratios in HIRs, like n/p [19], $t/^3$ He [20, 21], π^-/π^+ [22–25], K^0/K^+ [26] and Ξ^-/Ξ^0 [27], the $E_{\rm sym}(\rho)$ is still suffering a lot uncertainties [28–32], and the efforts are ongoing to search novel probes to explore the effects of $E_{\rm sym}(\rho)$ in HIRs [33–37].

The nuclear (fast) fission process is a large-amplitude collective motion mode happening in the HIRs. The low-density neutron-rich neck region formed in the rupture of two fission fragments provides a good condition for studying $E_{\rm sym}(\rho)$ and dynamic properties in isospin degree of freedom (IDOF)[38–41]. The neck zone has been explored to understand the mechanism of intermediate mass fragment (IMF) formation [42–45], isotopic cluster emission [46–49] and neutron-proton equilibration [50–54]. Because of the density gradient and the isospin migration, the neck zone provides a beneficial environment to study the $E_{\rm sym}(\rho)$ [52, 54]. For more discussions about neck zone, one can refer to the review articles of heavy ion reactions from the experimental [38, 39, 55] and theoretic points of view [56–60].



The emissions of light particles in coincidence with fission fragments are a natural idea for exploring the symmetry energy effect and (fast)fission properties in HIRs [40, 41]. Among the probes using the light charged particles (LCPs), the yield ratio of $t/^3$ He, written as $R(t/^3$ He), has been particularly identified to probe the enriched feature of isospin dynamics in HIRs. Transport model calculations demonstrate that the $R(t/^{3}\text{He})$ at intermediateenergy HIRs depends on the stiffness of $E_{\text{sym}}(\rho)$ [21, 61]. At high-energy HIRs, $R(t)^3$ He) depends more sensitively on the value of $E_{\text{sym}}(\rho)$ [62] and the specific form of the interaction potential [25, 63], but is less dependent on the slope of $E_{\text{sym}}(\rho)$ [64]. In addition, $R(t/^3\text{He})$ reflects the isospin-dependent nucleon density in the reactions [43, 65, 66]. Experimentally, the yield ratios of various mirror nucleus pairs, including the $R(t/^3He)$, led to the discovery of isospin fractionation [67]. It has been suggested that more neutron-rich particles are emitted at mid-rapidity, as inferred by the $R(t/^3He)$, which correlates positively with the charge number of projectile-like fragments[43] but reversely with the center of mass energy [68]. Similarly, in high-energies HIR, the $R(t/^3He)$ reflects the neutron enrichment of the emission source[43, 69, 70] and isospin mixing during the collision [71]. Recently, the $R(t/^3He)$ has also been used to study the pick-up mechanism of preequilibrium light nucleus production in the pion scattering experiment [72]. Hence, the distribution of $R(t/^3He)$ relative to the fission plane is a good probe to characterize the properties of fission process and explore the properties of symmetry energy.

Despite of the enormous progress of the studies on the triton (t) and ³He emission, some questions remain unclear and require further studies. For example, when considering the spectra of ³He, there is an anomalous phenomenon that the yield of high energy ³He is relatively larger, compared to that of triton [73-77] or ⁴He [73, 75-78]. This phenomenon has been called "³He-puzzle" [73, 74, 77]. While the energy spectra are suffering "3He-puzzle," the yield ratio of triton and ³He is sensitive to the neutron-to-proton ratio (N/Z) of the emitting system [53, 70, 79, 80]. The excitation function of $R(t/^3He)$ measured by the FOPI collaboration [81] cannot be reproduced with a single model [62]. More interestingly, the results of the INDRA experiment suggest that the triton and ³He isobars seem to dominate the neutron enrichment of the neck zone [54]. However, the existence of "3He-puzzle" in the coincidence events of LCPs and fission fragments is still an uncertain issue.

Due to the enriched but not-well-understood information carried by triton and ³He coupling to both the isospin transport and the neck emission during fission process in HIRs, we are motivated to explore the emission of these two isobars in coincidence with fission fragments by

inspecting the energy spectra and the yield ratio $R(t/^3 \text{He})$ over wide angular range, and to bridge the ratio $R(t/^3 \text{He})$ and the feature of fission process, as well as to infer the slope parameter of $E_{\text{sym}}(\rho)$. In this article, the energy spectra of triton and $^3 \text{He}$ in coincidence with fission fragments at different angles are measured in the reactions of $^{86}\text{Kr}+^{\text{nat}}\text{Pb}$ at 25 MeV/u. The distributions of $R(t/^3 \text{He})$ with respect to the fission plane and as a function of the laboratory polar angle are analyzed. The comparison of the experimental data to the transport model simulation is discussed. The paper is organized as following. Section 2 and 3 present the experimental setup and the description of the transport model, respectively. Section 4 shows the results and the discussions, and Sect. 5 shows the summary.

2 Experimental setup

The experiment was conducted at the Compact Spectrometer for Heavy IoN Experiment (CSHINE) [82, 83], built at the final focal plane of the Radioactive Ion Beam Line at Lanzhou (RIBLL-I) [84]. The ⁸⁶Kr beam of 25 MeV/u was extracted from the cyclotron of the Heavy Ion Research Facility at Lanzhou (HIRFL) [85], bombarding a natural lead target installed in the scattering chamber with the radius $R \approx 750$ mm. The target thickness is about 1 mg/cm². Figure 1 presents the experimental setup (a) and the spatial

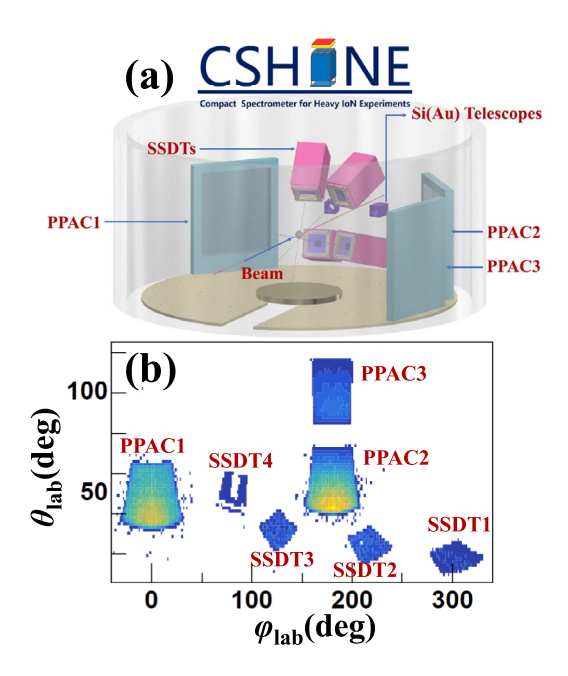


Fig. 1 (Color online) **a** The experimental setup of CSHINE. **b** The spatial coverage of SSDTs and PPACs on $\theta-\varphi$ plane in laboratory reference frame



coverage of the silicon-strip detector telescopes (SSDTs) and the parallel plate avalanche counters (PPACs) (b).

The LCPs from the reactions were measured by 4 SSDTs, covering the angular range from 10° to 60° in laboratory. Each SSDT consists of three layers, namely one single-sided silicon-strip detector (SSSSD) for ΔE_1 and one double-sided silicon-strip detector (DSSSD) for ΔE_2 , backed by a 3 × 3 CsI(Tl) crystal hodoscope with the length of 50 mm for the energy deposit E. The granularity of the SSDT is 4 mm \times 4 mm, giving about 1° angular resolution. The energy resolution of the SSDT is better than 2%, and the isotopes up to Z = 6 can be identified [36]. Multi-hits and signal sharing are carefully treated in the track recognition, and the track recognition efficiency is about 90% [86]. Figure 2 shows the particle identification of light particles for this analysis. Panel (a) to (d) presents the scattering plot of $\Delta E_2 - E_{CsI}$ of the four SSDTs. The results show that $Z \le 3$ LCPs, including triton and ³He, were identified clearly in each SSDT, supporting the reliability of the experimental results.

In order to explore the isospin properties of fission process, the fission fragments (FFs) were detected by 3 PPACs, each of which had a sensitive area of 240 mm × 280 mm [87, 88]. The perpendicular distance of the PPACs to the target is about 428 mm. The coverage of the PPACs ensures a high efficiency to measure the FFs in coincidence with the LCPs. And the trigger system is established to select the fission events [89]. The working voltage of the PPACs can suppress the light charged particles significantly, although the specific values of mass and charge for FFs were not accurately determined. According to the previous source test results [82], the detection efficiency is almost 100% for FFs and negligibly low for light particles with the detector condition (HV=460 V) as adopted in the experiment. So, the PPACs can only be fired by heavy fragments, rather than LCPs or IMFs.

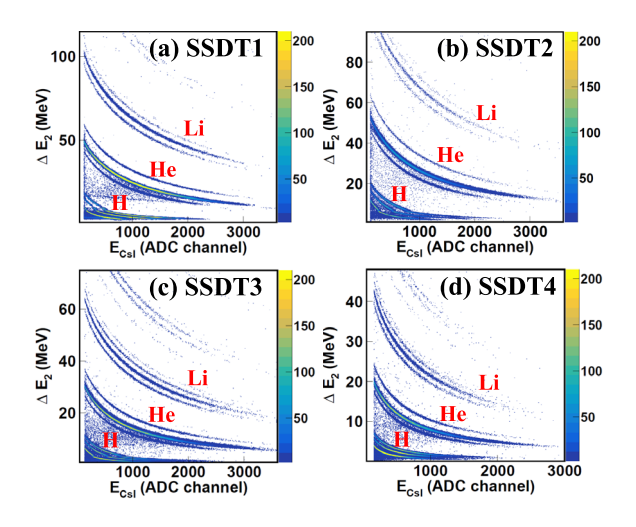


Fig. 2 (Color online) $\Delta E_2 - E_{\text{CsI}}$ plots of the four SSDTs

Referring to the energy loss calculations only, the projectile-like fragments (PLFs) and target-like fragments (TLFs) may fire the PPACs as well. However, the geometric coverage of the PPACs in the experiment suppresses the PLF and TLF. Otherwise because PLFs and TLFs are well separated in velocity ($v_{\rm PLF} \approx 6.8~{\rm cm/ns}, v_{\rm TLF} \approx 1.2~{\rm cm/ns}$ at small linear momentum transfer or in peripheral reactions), one shall be able to see two components clearly on the velocities of the two-coincident fragments recorded in the PPACs. Indeed, the two-component feature is not visible in the velocity scattering plot (see Fig. 11 in [87]), and it is safe and reasonable to speculate that the heavy fragments detected with PPACs in the experiment are mainly fission fragments.

3 Theoretical model

A hybrid model by the improved quantum molecular dynamics model (ImQMD05) coupled with statistical decay afterburner (GEMINI) was used for theoretical simulation in this work. The ImQMD05 [90] was used to simulate the nucleon transport process in HIRs. And the GEMINI [91, 92] was appended to obtain the final state productions of the reactions. The ImQMD05 model is an improved version from the original quantum molecular dynamics code [93, 94] and is widely used to understand the dynamics of nuclear reactions induced by heavy ions or light nuclei at both low and intermediate energies [40, 41, 95–97]. The mean field part of the ImQMD05 model used here includes the symmetry potential energy part. And the local nuclear potential energy density functional in the ImQMD05 model is written as

$$V_{\text{loc}} = \frac{\alpha}{2} \frac{\rho^2}{\rho_0} + \frac{\beta}{\eta + 1} \frac{\rho^{\eta + 1}}{\rho_0^{\eta}} + \frac{g_{\text{sur}}}{2\rho_0} (\nabla \rho)^2 + \frac{g_{\text{sur,iso}}}{\rho_0} [\nabla (\rho_n - \rho_p)]^2 + g_{\rho\tau} \frac{\rho^{8/3}}{\rho_0^{5/3}} + \frac{C_s}{2} \frac{\rho^{\gamma + 1}}{\rho_0^{\gamma}} \delta^2,$$
(1)

where ρ , $\rho_{\rm n}$ and $\rho_{\rm p}$ are the density of nucleon, neutron and proton, respectively. $\delta = (\rho_{\rm n} - \rho_{\rm p})/(\rho_{\rm n} + \rho_{\rm p})$ is the isospin asymmetry degree. The parameters in Eq. (1) except $C_{\rm s}$, which are listed in Table 1, are obtained directly from Skyrme interaction with MSL0 parameter set [98]. $C_{\rm s}$ is determined by the symmetry potential energy at saturation density. Together with different values of γ , one can get the MSL0-like Skyrme interaction with various density-dependent symmetry potential energy. After scanning the impact parameter up to 16.0 fm, the most probable weight of the fission events filtered by experimental conditions is located at 7.0 fm. Hence, the reaction was simulated with impact parameter in the range of $1.0 \le b \le 7.0$ fm by a step of $\Delta b = 1.5$ fm. At the end of the dynamical evolution in ImQMD05, setting at 500 fm/c, the minimum spanning tree



155 Page 4 of 12 Y.-J. Wang et al.

Table 1 Parameter set used in the ImQMD05 calculations

α (MeV)	β (MeV)	η	g _{sur} (MeV fm ²)	g _{sur,iso} (fm ²)	$g_{ ho au}$ (MeV)	C _s (MeV)	ρ_0 (fm ⁻³)
-254	185	5/3	21.0	-0.82	5.51	36.0	0.160

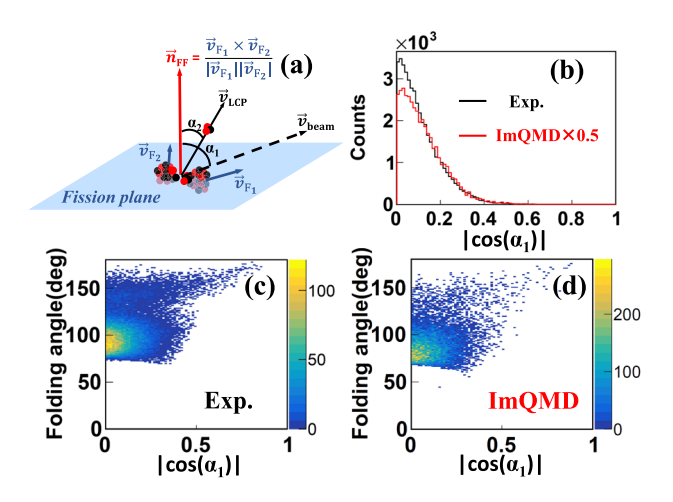


Fig. 3 (Color online) **a** Geometric diagram of fission plane of FFs and LCP emission. **b** Angular distribution between the normal vector \vec{n}_{FF} of the fission plane and the beam direction \vec{v}_{beam} . The experimental **c** and simulation **d** results of the folding angle $vs. |\cos(\alpha_1)|$ are shown in the bottom panels

(MST) algorithm [94, 99] was used to recognize the free nucleons and fragments formed in the evolution. Next, the statistical decay of excited fragments was performed with GEMINI afterburner. At last, the information of final state particles will be obtained.

4 Results and discussion

4.1 Characterizing the fission events

We start with the analysis of the orientation of the fission plane with respect to the beam direction. The fission plane is reconstructed by the velocity of two FFs, using $\vec{n}_{FF} = (\vec{v}_{F_1} \times \vec{v}_{F_2})/|\vec{v}_{F_1}||\vec{v}_{F_2}|$ to denote the normal vector of the fission plane, as shown in Fig. 3a. Defining α_1 as the angle between \vec{n}_{FF} and the beam direction \vec{v}_{beam} , one can characterize how much the fission plane deviates from the beam. The distribution of $|\cos(\alpha_1)|$ is peaked at 0 with a rather small width $\sigma_{\alpha_1} \approx 6^\circ$, as shown in Fig. 3b, inferring that the fission plane keeps approximately the memory of the initial angular momentum of the rotating system. With $Z \ge 10$ as the condition to identify FFs for theoretical calculations, the transport model prediction about the distribution of $|\cos(\alpha_1)|$ is in rather agreement with the experiment. The scattering plots of folding angle $vs. |\cos(\alpha_1)|$ provide

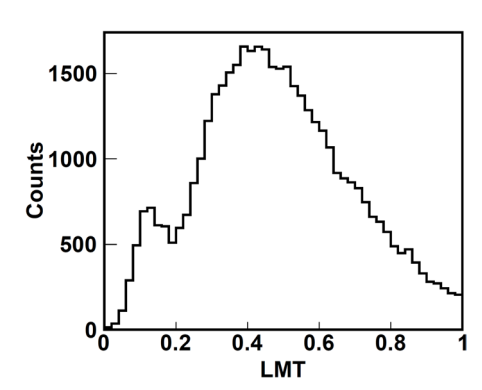


Fig. 4 Experimental distribution of LMT

the information of fission and detection geometry. With the detector filter of PPACs on both θ_{lab} and ϕ_{lab} according to the setup, the experimental folding angle in Fig. 3c can be approximately described by the model simulation in Fig. 3d.

The characteristics of this rotating fissioning system was obtained using the experiment data and theoretic simulations. First, to estimate its charge and mass, the linear momentum transfer (LMT) should be estimated experimentally. Assuming a symmetric fission processes, the velocity of the fissioning system (FS) can be simply calculated by

$$\vec{v}_{FS} = \frac{1}{2}(\vec{v}_{F1} + \vec{v}_{F2}),\tag{2}$$

where \vec{v}_{F1} and \vec{v}_{F2} are the velocities of the two FFs, respectively. The LMT is defined as

$$LMT = \frac{A_{tar} \cdot v_{FS}^Z}{A_{pro} \cdot (v_{pro} - v_{FS}^Z)}.$$
 (3)

Here, the subscripts pro and tar denote the projectile and the target, respectively. v_{FS}^Z is the projection of \vec{v}_{FS} on the beam direction. As shown in Fig. 4, the distribution of the LMT derived from the experimental data is peaked in the vicinity of 0.4. The small peak below LMT < 0.2 is contributed by the fission events triggered by PPAC 1 and PPAC 3. Accordingly, the typical charge and mass of the rotating fission system are $Z_{FS} \approx Z_{tar} + Z_{pro} \cdot LMT = 96$ and $A_{FS} \approx A_{tar} + A_{pro} \cdot LMT = 242$.

Second, to estimate the angular momentum of the rotating fission system, one needs the most probable impact parameter, which can determined by the event weigh obtained from transport model simulations filtered by experimental conditions. Define the fission event weight by



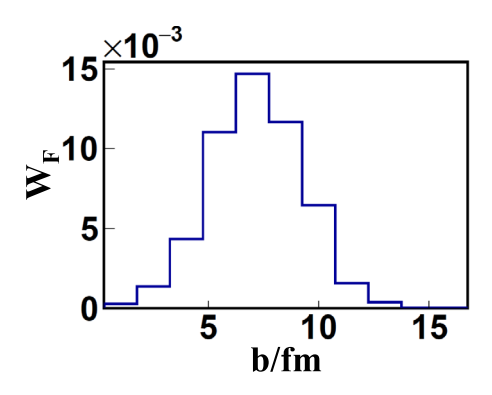


Fig. 5 The weight of the fission events as a function of impact parameter b in ImQMD05 simulations

$$W_{\rm F} = b \frac{n_{\rm F}}{N_{\rm tot}(b)},\tag{4}$$

where $n_{\rm F}$ is the number of fission events among $N_{\rm tot}$ events simulated at a given impact parameter b.

Figure 5 shows the distribution of $W_{\rm F}$, where the most probable impact parameter $b_{\rm m}$ is located in the vicinity of 7 fm.

The distance between the transferred part of the projectile and the mass center of the fissioning system is defined as

$$D = b_{\rm m} \frac{A_{\rm tar}}{A_{\rm tar} + A_{\rm pro} \cdot \rm LMT}, \tag{5}$$

where $b_{\rm m}=7$ fm, $A_{\rm tar}=208$, $A_{\rm pro}=86$ and LMT = 0.4, respectively.

The angular momentum is written as

$$J = P_{\text{pro}} \cdot \text{LMT} \cdot D, \tag{6}$$

where $P_{\rm pro}=18700~{\rm MeV}/c$ and $D\approx 6~{\rm fm}$ was derived with LMT = 0.4. Then, the angular momentum of the rotating system is approximately $J\approx 200~\hbar$.

Third, to estimate the excitation energy of the rotating fission system, the moment of inertia I of a spherical nucleus with the mass $M_{\rm FS}$ is

$$I = \frac{2}{5}M_{\rm FS}r_{\rm FS}^2,\tag{7}$$

where $r_{\rm FS} = 1.4 A_{\rm FS}^{1/3}$ fm is the radius of the fissioning system. The rotating energy $E_{\rm rot} = J^2/2I \approx 100$ MeV is approximately obtained. Ignoring the reaction Q value, the excitation energy could be extracted by

$$E^* = E_{\rm kin}^{\rm i} - E_{\rm kin}^{\rm f} - E_{\rm rot}, \tag{8}$$

where $E_{\rm kin}^{\rm i}$ and $E_{\rm kin}^{\rm f}$ are the initial state kinetic energy and the final state kinetic energy, respectively. Approximately, one has $E^* \approx 600$ MeV. The excitation energy is close to the one of the fission system formed in 25 MeV/u Ar+Au at

LMT \approx 80%, where the E^* was calculated by the pre-scission α multiplicity [100]. For additional properties of fission systems, such as Viola systematics and angular distribution of the fission axis, please refer to our previously published paper [87].

4.2 Analysis of the energy spectra of t and ³He

We now present the analysis of the emission of triton and ³He in the (fast)fission events. The energy spectra of LCPs in coincidence with FFs contain thermal and dynamical information of the particles emitted from the fission events. Figure 6 presents the energy spectra of triton (open circles) and ³He (open triangles) emitted from fission events in different angular ranges corresponding to SSDTs 2 to 4. To reduce the contamination of quasi-projectiles, the data of SSDT1 covering $10 - 20^{\circ}$ in the laboratory are not counted here. It is shown that the spectrum of ³He is generally harder than that of triton, leading to a larger average kinetic energy of the former. The difference between triton and ³He is more pronounced at forward angles than at large angles. This observation of "³He-puzzle" is in accordance with the previous inclusive measurements at high beam energies [73, 75–77, 81, 101-104].

The "³He-puzzle" has been interpreted by two possible scenarios: sequential decay [74] and coalescence model [78]. In the sequential decay scenario, the difference between ³He and triton is influenced by the Coulomb barrier, for which ³He is emitted at an earlier stage with high temperature to overcome the Coulomb barrier higher than that of triton [74]. In coalescence scenario, which was applied to interpret the difference between ³He and α particles [78], the former is dominantly produced by the coalescence of pre-equilibrium nucleons, delivering larger mean kinetic energy. These two explanations are qualitatively in agreement, supporting that ³He is predominantly emitted at earlier stage. Our experimental results show that the "³He-puzzle" exists in the events tagged by fission.

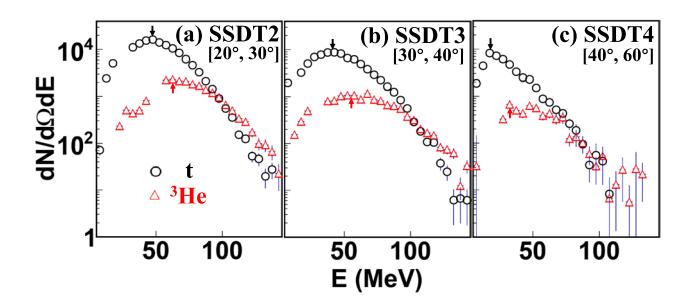


Fig. 6 (Color online) The experimental energy spectra of triton (circle) and 3 He (triangle) in $20^\circ \le \theta_{lab} \le 60^\circ$ covered by SSDT2 to SSDT4 in coincidence with two FFs. The arrows represent the peak position of each experimental energy spectrum



155 Page 6 of 12 Y.-J. Wang et al.

It suggests that the puzzle exists in both inclusive and fission events

4.3 Out-of-plane emission and the effect of $E_{\text{sym}}(\rho)$

Benefiting from the wide angular coverage of the SSDTs and PPACs in laboratory reference frame, the angular behavior of the particle emission can be analyzed. To compare the yields of particles with different energy spectrum behaviors and avoid the influence of the possible experimental distortion caused by the energy threshold in each SSDTs, a data adaptive energy spectrum peak cut scenario is applying. We focus on the descending part on the high-energy side of the energy peak. The energy peak positions $(E_{\rm p})$ are listed in Table 2. Meanwhile, using the energy condition $E \geq E_{\rm p}$ as the low limit cut, one can suppress the interference of the evaporation process and emphasize the feature of the dynamic emission.

The angular distribution of $R(t/^3\text{He})$ as a function of the polar angle in laboratory θ_{lab} is generated with events of one LCP in coincidence with two FFs, as shown in Fig. 7. The same energy threshold, geometry, and folding angle cuts are applied to both experimental and simulation results. It is shown that for the wide angular range, the distribution exhibits a rising trend. This feature is consistent with the moving source picture, where the neutron richness of particle emission increases from the projectile-like source to the medium-velocity source corresponding to the neck, as predicted by various transport model simulations [40, 41, 46, 48, 49, 51, 105–109], and experimentally observed in a specific angular window [42, 45, 50, 54, 79, 110–112] or a parallel velocity window [45, 79, 80, 113–118].

In order to see the symmetry energy effect, a soft ($\gamma = 0.5$) and a stiff ($\gamma = 1.0$) symmetry energy are adopted in the ImQMD05 simulations. These two γ values correspond to slope parameter of $E_{\rm sym}(\rho)$ with L = 51 and 77 MeV at ρ_0 , respectively. Although the predicted value of $R(t/^3{\rm He})$ is far off to the experiment, the rising trend of $R(t/^3{\rm He})$ as a function of $\theta_{\rm lab}$ was reproduced by model simulations in both γ cases. In order to quantify the increasing rate, the function of $f(x) = e^{(p_0 + p_1 x)}$ is applied to fit the data and the model predictions, respectively. The parameter p_1 describes the increasing rate of $R(t/^3{\rm He})$ to $\theta_{\rm lab}$. As shown in Fig. 7, the rising trend depends on γ . Visibly, a softer $E_{\rm sym}(\rho)$ causes a relative larger increasing rate. When comparing the fitting results between experiment and model in Table 3, the value of experimental p_1 is marginally located between $\gamma = 0.5$ and 1.0. Nevertheless,

Table 2 Energy peak position E_p of triton and ³He for SSDT 2 to 4

	SSDT2	SSDT3	SSDT4
$E_{\rm p}$ of triton (MeV)	45	40	19
$E_{\rm p}$ of $^{3}{\rm He}$ (MeV)	62	58	38

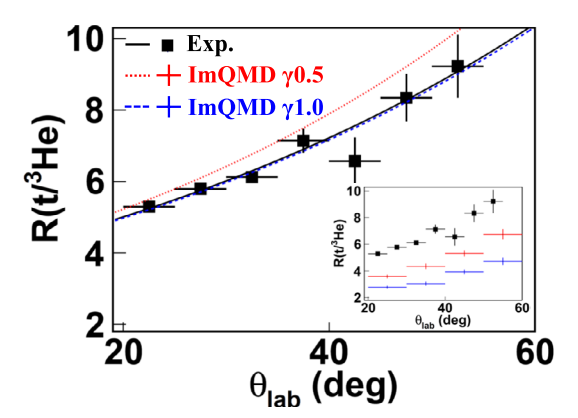


Fig. 7 (Color online) The ratio $R(t/^3{\rm He})$ as a function of $\theta_{\rm lab}$. The black solid squares and black line represent the experiment data and fitting result with $E \ge E_{\rm p}$ cuts in coincidence with fission events. The red and blue cross markers represent the ImQMD05 calculations data of $\gamma=0.5$ and 1.0 in the inset. The red dot and blue dash lines are the fitting results of $\gamma=0.5$ and 1.0 which is normalized with experimental fitting result of p_0

the large uncertainty here reduces the sensitivity and hinder to make a convincing constraint of $E_{\text{sym}}(\rho)$.

It is then motivated to go a further step to find a novel probe, of which the fission event topology is better controlled and the sensitivity on $E_{\text{sym}}(\rho)$ can be enhanced. Figure 8 presents the angular distribution of $R(t/^3He)$ with respect to the fission plane. The α_2 on the abscissa is the relative angle between $\vec{n}_{\rm FF}$ and the velocity of the coincident triton or ${}^{3}\text{He }\vec{v}_{\text{LCP}}$ as shown in Fig. 3a, with $|\cos(\alpha_2)| = 0$ (1) corresponding to in-plane (out-of-plane) emission. Again, the same cuts are applied for both experimental and theoretical results. The increasing trend of $R(t/^3\text{He})$ with $|\cos(\alpha_2)|$ indicates that the neutron-rich particles emitted from out-of-fission-plane is enhanced. This phenomenon is the consequence of the competition between the isospin migration and the centrifugal motion of the particles in the rotating fission system. When the reaction system is viewed as a rotating emission source, particles emitted near the fission plane are subjected to stronger centrifugal potential during the emission process, weakening the difference between neutrons and protons under the isovector potential. From the in-plane to out-of-plane, more neutron-rich particles are emitted due to the effect of isospin fractionation [67], indicating that the effect of the isovector potential becomes more significant compared to centrifugal potential. This observation gives

Table 3 Fitting results of the ratio $R(t/^3\text{He})$ as a function of θ_{lab} using $f(x) = e^{(p_0 + p_1 x)}$

	p_0	p_1
Experiment	1.25±0.06	0.018±0.002
$\gamma = 0.5$	0.75 ± 0.08	0.021 ± 0.002
$\gamma=1.0$	0.54 ± 0.09	0.018 ± 0.002



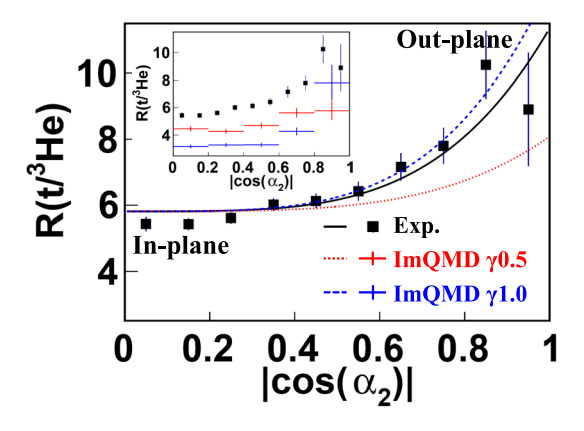


Fig. 8 (Color online) The ratio $R(t/^3He)$ as a function of $|\cos(\alpha_2)|$. The black solid squares and black line represent the experiment data and fitting result. The red and blue cross markers represent the theoretical calculations data of $\gamma = 0.5$ and 1.0 in the inset. The red dot and blue dash lines are the fitting results of $\gamma = 0.5$ and 1.0 which is normalized with experimental fitting result of p_0

us the chance to explore the properties of isospin transport and the density dependence of $E_{\text{sym}}(\rho)$ in (fast)fission reactions.

Similarly, to describe the increasing trend of the angular distribution of $|\cos(\alpha_2)|$, the function of $f(x) = p_0 + p_1 x^4$ is used to fit data and the simulations. Again, p_0 is far off to the experiment due to the clustering difficulty of transport model, but the parameter p_1 can be used to describe the increasing rate of the ratio with out-of-plane angle. In Fig. 8, the fitting curves exhibit a different increasing behavior between $\gamma = 0.5$ and 1.0, indicating that the enhancement of neutron-rich particle emission out-of-fission-plane is sensitive to the form of $E_{\text{sym}}(\rho)$. Inspecting the increasing curves and the values of p_1 as listed in Table 4, one finds that the experimental increasing rate situates between the theoretical prediction with $\gamma =$ 0.5 and 1.0, in accordance with the conclusion of our previous work [36], where a totally different probe was used. The comparison seems to exclude very soft (γ <0.5) and very stiff $(\gamma > 1.0)$ candidates of symmetry energy. The results indicate that the ratio $R(t/^3\text{He})$ as a function of $|\cos(\alpha_2)|$ seems to be a sensitive probe for density-dependent symmetry energy, especially in the larger $|\cos(\alpha_2)|$ range, which is very close to the boundary of the current detector coverage. Hence, more events in the larger $|\cos(\alpha_2)|$ range are preferentially requested in the further experiments. Data analysis of a new measurement of 86 Kr $+^{124}$ Sn at 25 MeV/u is ongoing [119].

Table 4 Fitting results of $R(t/^3He)$ as a function of $|\cos(\alpha_2)|$ using $f(x) = p_0 + p_1 x^4$

	p_0	p_1
Experiment	5.8±0.2	5.5±1.6
$\gamma = 0.5$	4.5 ± 0.1	2.3 ± 1.1
$\gamma = 1.0$	3.0 ± 0.1	6.8 ± 1.8

Figure 9 shows in addition the relationship between $|\cos(\alpha_2)|$ and θ_{lab} with the experiment events of triton in coincidence with two fission fragments. Visibly, there is a weak positive correlation between $|\cos(\alpha_2)|$ and θ_{lab} . The origin of the correlation is partly due to the fact that the azimuth coverage of the PPAC is quite limited. With such weak correlation, one infers that the two distributions shown in Figs. 7 and 8 have their own implications. Namely, the distribution of $R(t/^3\text{He})$ as a function of θ_{lab} indicates that the low-density and neutron-rich medium-velocity emission source (neck) is formed, while the distribution of $R(t/^{3}\text{He})$ as a function of $|\cos(\alpha_{2})|$ characterizes the fine out-of-plane properties of the isospin transport in a fissioning process. Upon comparing the results presented in Table 3 and Table 4, it becomes evident that the enhancement of $R(t/^3\text{He})$ vs. $|\cos(\alpha_2)|$, particularly at larger out-of-plane angles, appears to be a more sensitive probe for studying nuclear symmetry energy than the polar angular distribution of $R(t/^3He)$. In another word, in the properly characterized fission events, the effect of $E_{\rm sym}(\rho)\,$ can be magnified, supporting the previous predictions by transport model simulations [40].

Currently, we do not attempt to make a fine tuning and constraint of γ parameter in the simulations, since the absolute value of $R(t/^3He)$ is not yet well reproduced, as indicated in Figs. 7 and 8. Further studies are required in transport model in order to elucidate the origin and the formation mechanism of light clusters including triton and ³ He. Recently, the yield of light clusters is better reproduced by introducing Mott effect in transport model [120]. Meanwhile, the cooling process of the rotating fissioning system with similar E^* and J is of high interest. We are going to make further calculations on particle emission from a rotating system with inclusion of deuteron, triton and ³He apart of neutron, proton and α particles, as done in [121]. The

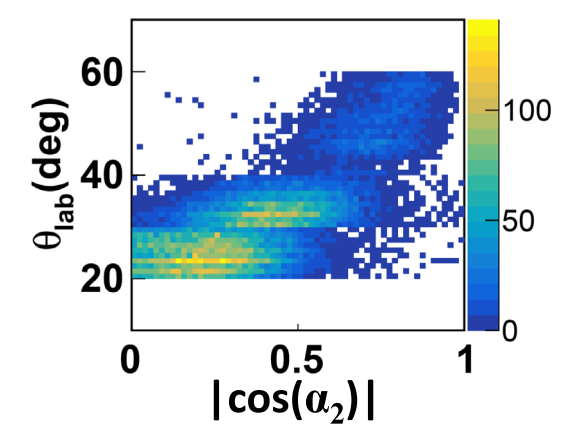


Fig. 9 (Color online) The scattering plot between $|\cos(\alpha_2)|$ and laboratory angle with the experiment events of triton in coincidence with two fission fragments



emission of other particles than A=3 isobars may bring significant effect to the featured distribution of the latter in the cooling process of the fissioning system.

5 Summary

The energy spectra and angular distributions of triton and ³He ranging from 20° to 60° in the laboratory in coincidence with fission fragments are analyzed in 25 MeV/u ⁸⁶Kr + ^{nat}Pb reactions. It is shown that the energy spectra of ³He are generally harder than triton even in the fission events, and the effect is more pronounced at small angles. Applying a data-driven energy spectrum peak cut scenario, the rising trend of angular distribution of $R(t/^3He)$ is observed in the coincident events of one LCP and two FFs, which is consistent with previous inclusive observations. The yield ratio $R(t/^3\text{He})$ exhibits an enhancement as a function of $|\cos(\alpha_2)|$, evidencing more neutron-rich particles emitted from out-offission-plane. With a qualitative comparison with ImOMD05 simulations, the enhancement of neutron-rich particle emission from out-of-fission-plane seems to be a novel probe for nuclear symmetry energy. More measurements at large outof-fission-plane angles and further theoretic investigations are required for a stringent constraint of $E_{\text{sym}}(\rho)$.

Acknowledgements The authors thank Huigan Cheng from SCUT, Zhen Zhang from SYSU and Rui Wang from INFN for their valuable discussions.

Author Contributions All authors contributed to the study conception and design. Material preparation, data collection and analysis were performed by Yi-Jie Wang. Theoretical calculation and analysis were performed by Meng-Ting Wan and Yi-Jie Wang. The project was leaded and supervised by Yi-Jie Wang, Li Ou and Zhi-Gang Xiao. The first draft of the manuscript was written by Yi-Jie Wang, and all authors commented on previous versions of the manuscript. All authors read and approved the final manuscript.

Data Availability The data that support the findings of this study are openly available in Science Data Bank at https://cstr.cn/31253.11.sciencedb.j00186.00707 and https://doi.org/10.57760/sciencedb.j00186.00707.

Declarations

Conflict of interest Chun-Wang Ma and Hong-Wei Wang are editorial board members for Nuclear Science and Techniques and were not involved in the editorial review, or the decision to publish this article. All authors declare that there are no conflict of interest.

References

 B.A. Li, B.J. Cai, W.J. Xie et al., Progress in constraining nuclear symmetry energy using neutron star observables since GW170817. Universe 7(6), 182 (2021). https://doi.org/10.3390/ universe7060182

- S. Huth, P.T.H. Pang, I. Tews et al., Constraining neutron-star matter with microscopic and macroscopic collisions. Nature 606, 276–280 (2022). https://doi.org/10.1038/s41586-022-04750-w
- A.W. Steiner, M. Prakash, J.M. Lattimer et al., Isospin asymmetry in nuclei and neutron stars. Phys. Rept. 411, 325–375 (2005). https://doi.org/10.1016/j.physrep.2005.02.004
- M. Oertel, M. Hempel, T. Klähn et al., Equations of state for supernovae and compact stars. Rev. Mod. Phys. 89, 015007 (2017). https://doi.org/10.1103/RevModPhys.89.015007
- B.A. Li, A. Ramos, G. Verde et al., Topical issue on nuclear symmetry energy. Eur. Phys. J. A 50, 9 (2014). https://doi.org/ 10.1140/epja/i2014-14009-x
- B.A. Li, L.W. Chen, C.M. Ko, Recent progress and new challenges in isospin physics with heavy-ion reactions. Phys. Rept. 464, 113–281 (2008). https://doi.org/10.1016/j.physrep.2008.04. 005
- B.P. Abbott et al., [LIGO Scientific and Virgo], GW170817: observation of gravitational waves from a binary neutron star inspiral. Phys. Rev. Lett. 119, 161101 (2017). https://doi.org/10. 1103/PhysRevLett.119.161101
- B.P. Abbott et al., [LIGO Scientific and Virgo], GW170817: measurements of neutron star radii and equation of state. Phys. Rev. Lett. 121, 161101 (2018). https://doi.org/10.1103/PhysRevLett.121.161101
- S. De, D. Finstad, J.M. Lattimer, D.A. Brown et al., Tidal deformabilities and radii of neutron stars from the observation of GW170817. Phys. Rev. Lett. 121, 091102 (2018). https://doi. org/10.1103/PhysRevLett.121.091102
- M.Q. Ding, D.Q. Fang, Y.G. Ma, Neutron skin and its effects in heavy-ion collisions. Nucl. Sci. Tech. 35, 211 (2024). https://doi. org/10.1007/s41365-024-01584-1
- T.Z. Yan, S. Li, Isotopic dependence of the yield ratios of light fragments from different projectiles and their unified neutron skin thicknesses. Nucl. Sci. Tech. 35, 65 (2024). https://doi.org/ 10.1007/s41365-024-01425-1
- W.J. Xie, Z.W. Ma, J.H. Guo, Bayesian inference of the crustcore transition density via the neutron-star radius and neutronskin thickness data. Nucl. Sci. Tech. 34, 91 (2023). https://doi. org/10.1007/s41365-023-01239-7
- D.Q. Fang, Neutron skin thickness and its effects in nuclear reactions. Nucl. Tech. (in Chinese) 46, 080016 (2023). https://doi.org/10.11889/j.0253-3219.2023.hjs.46.080016
- R. An, S. Sun, L.G. Cao et al., New quantification of symmetry energy from neutron skin thicknesses of ⁴⁸Ca and ²⁰⁸ Pb. Nucl. Sci. Tech. 35, 182 (2024). https://doi.org/10.1007/s41365-024-01551-w
- R. An, S. Sun, L.G. Cao et al., Constraining nuclear symmetry energy with the charge radii of mirror-pair nuclei. Nucl. Sci. Tech. 34, 119 (2023). https://doi.org/10.1007/s41365-023-01269-1
- F.P. Li, L.G. Pang, X.N. Wang, Application of machine learning to the study of QCD transition in heavy ion collisions. Nucl. Tech. (in Chinese) 46, 040014 (2023). https://doi.org/10.11889/j. 0253-3219.2023.hjs.46.040014
- Y.Y. Liu, J.P. Yang, Y.J. Wang et al., A perspective on describing nucleonic flow and pionic observables within the ultra-relativistic quantum molecular dynamics model. Nucl. Sci. Tech. 36, 45 (2025). https://doi.org/10.1007/s41365-024-01607-x
- S.N. Wei, Z.Q. Feng, Properties of collective flow and pion production in intermediate-energy heavy-ion collisions with a relativistic quantum molecular dynamics model. Nucl. Sci. Tech. 35, 15 (2024). https://doi.org/10.1007/s41365-024-01380-x
- B.A. Li, C.M. Ko, Z.Z. Ren, Equation of state of asymmetric nuclear matter and collisions of neutron rich nuclei. Phys. Rev. Lett. 78, 1644 (1997). https://doi.org/10.1103/PhysRevLett.78. 1644



- 20. Y.X. Zhang, Z.X. Li, Probing the density dependence of the symmetry potential with peripheral heavy-ion collisions. Phys. Rev. C 71, 024604 (2005). https://doi.org/10.1103/PhysRevC. 71.024604
- 21. L.W. Chen, C.M. Ko, B.A. Li, Light clusters production as a probe to the nuclear symmetry energy. Phys. Rev. C 68, 017601 (2003). https://doi.org/10.1103/PhysRevC.68.017601
- 22. B.A. Li, Probing the high density behavior of nuclear symmetry energy with high-energy heavy ion collisions. Phys. Rev. Lett. 88, 192701 (2002). https://doi.org/10.1103/PhysRevLett. 88.192701Li:2002qx
- 23. Z. Xiao, B.A. Li, L.W. Chen et al., Circumstantial evidence for a soft nuclear symmetry energy at suprasaturation densities. Phys. Rev. Lett. 102, 062502 (2009). https://doi.org/10.1103/ PhysRevLett.102.062502
- 24. J. Estee et al., [SpiRIT], Probing the symmetry energy with the spectral pion ratio. Phys. Rev. Lett. 126, 162701 (2021). https://doi.org/10.1103/PhysRevLett.126.162701
- 25. Q. Li, Z. Li, S. Soff et al., Probing the density dependence of the symmetry potential at low and high densities. Phys. Rev. C 72, 034613 (2005). https://doi.org/10.1103/PhysRevC.72. 034613
- 26. G. Ferini, T. Gaitanos, M. Colonna et al., Isospin effects on subthreshold kaon production at intermediate energies. Phys. Rev. Lett. 97, 202301 (2006). https://doi.org/10.1103/PhysRevLett.
- 27. G.C. Yong, B.A. Li, Z.G. Xiao et al., Probing the high-density nuclear symmetry energy with the Ξ -/ Ξ 0 ratio in heavy-ion collisions at sNN≈3 GeV. Phys. Rev. C 106, 024902 (2022). https:// doi.org/10.1103/PhysRevC.106.024902
- 28. J. Xu, Transport approaches for the description of intermediateenergy heavy-ion collisions. Prog. Part. Nucl. Phys. 106, 312-359 (2019). https://doi.org/10.1016/j.ppnp.2019.02.009
- 29. Y.J. Wang, Q.F. Li, Application of microscopic transport model in the study of nuclear equation of state from heavy ion collisions at intermediate energies. Front. Phys. (Beijing) 15, 44302 (2020)
- 30. Y.X. Zhang, Y.J. Wang, M. Colonna et al., [TMEP], Comparison of heavy-ion transport simulations: collision integral in a box. Phys. Rev. C 97, 034625 (2018). https://doi.org/10.1103/PhysR evC.97.034625
- 31. A. Ono, J. Xu, Maria Colonna et al., [TMEP], Comparison of heavy-ion transport simulations: collision integral with pions and Δ resonances in a box. Phys. Rev. C 100, 044617 (2019). https:// doi.org/10.1103/PhysRevC.100.044617
- 32. M. Colonna, Y.X. Zhang, Y.J. Wang et al., [TMEP], Comparison of heavy-ion transport simulations: mean-field dynamics in box. Phys. Rev. C 104, 024603 (2021). https://doi.org/10.1103/PhysR evC.104.024603
- 33. Y. Zhang, J. Tian, W. Cheng et al., Long-time drift of the isospin degree of freedom in heavy ion collisions. Phys. Rev. C 95, 041602 (2017). https://doi.org/10.1103/PhysRevC.95.041602
- 34. L. Ou, Z. Xiao, H. Yi et al., Dynamic isovector reorientation of deuteron as a probe to nuclear symmetry energy. Phys. Rev. Lett. 115, 212501 (2015). https://doi.org/10.1103/PhysRevLett.115.
- 35. Y. Wang, F. Guan, Q. Wu et al., The emission order of hydrogen isotopes via correlation functions in 30 MeV/u Ar+Au reactions. Phys. Lett. B 825, 136856 (2022). https://doi.org/10.1016/j.physl etb.2021.136856
- 36. Y. Wang, F. Guan, X. Diao et al., Observing the ping-pong modality of the isospin degree of freedom in cluster emission from heavy-ion reactions. Phys. Rev. C 107, L041601 (2023). https://doi.org/10.1103/PhysRevC.107.L041601
- 37. Y. Wang, Z. Xiao, Correlation function studies at intermediate energies at CSHINE. Il. Nuovo. Cimento. C 48, 37 (2025). https://doi.org/10.1393/ncc/i2025-25037-x

- 38. G. Poggi, Neck emissions and the isospin degree of freedom. Nucl. Phys. A 685, 296-311 (2001). https://doi.org/10.1016/ \$0375-9474(01)00548-6
- 39. M.D. Toro, A. Olmi, R. Roy, Neck dynamics. Eur. Phys. J. A 30, 65-70 (2006). https://doi.org/10.1140/epja/i2006-10106-9
- 40. O. Wu, F. Guan, X. Diao et al., Symmetry energy effect on emissions of light particles in coincidence with fast fission. Phys. Lett. B 811, 135865 (2020). https://doi.org/10.1016/j. physletb.2020.135865
- 41. Q. Wu, X. Diao, F. Guan et al., Transport model studies on the fast fission of the target-like fragments in heavy ion collisions. Phys. Lett. B **797**, 134808 (2019). https://doi.org/10.1016/j. physletb.2019.134808
- 42. J. Toke, B. Lott, S.P. Baldwin et al., Intermediate-mass fragment decay of the neck zone formed in peripheral ²⁰⁹Bi + ¹³⁶Xe collisions at $E_{lab}/A=28$ MeV. Phys. Rev. Lett. **75**, 2920–2923 (1995). https://doi.org/10.1103/PhysRevLett.75.2920
- 43. J.F. Dempsey, R.J. Charity, L.G. Sobotka et al., Isospin dependence of intermediate mass fragment production in heavy-ion collisions at E/A=55 MeV. Phys. Rev. C **54**, 1710–1719 (1996). https://doi.org/10.1103/PhysRevC.54.1710
- 44. E. Ramakrishnan, H. Johnston, F. Gimeno-Nogues et al., Fragment emission from the mass-symmetric reactions 58 Fe, 58 Ni + 58 Fe 58 Ni at $E_{\text{beam}} = 30$ MeV/nucleon. Phys. Rev. C 57, 1803–1811 (1998). https://doi.org/10.1103/PhysRevC.
- 45. S. Hudan, R. Alfaro, B. Davin et al., Comparison of midvelocity fragment formation with projectile-like decay. Phys. Rev. C 71, 054604 (2005). https://doi.org/10.1103/PhysRevC.
- 46. L.G. Sobotka, J.F. Dempsey, R.J. Charity et al., Clustered and neutron-rich low density 'neck' region produced in heavy-ion collisions. Phys. Rev. C 55, 2109-2111 (1997). https://doi.org/ 10.1103/PhysRevC.55.2109
- 47. R. Laforest, E. Ramakrishnan, D.J. Rowland et al., Dependence of projectile fragmentation on target N/Z. Phys. Rev. C 59, 2567-2573 (1999). https://doi.org/10.1103/PhysRevC.59.2567
- 48. Y. Zhang, C. Zhou, J. Chen et al., Correlation between the fragmentation modes and light charged particles emission in heavy ion collisions. Sci. China Phys. Mech. Astron. 58, 112002 (2015). https://doi.org/10.1007/s11433-015-5723-2
- 49. Z.Q. Feng, Effects of isospin dynamics on neck fragmentation in isotopic nuclear reactions. Phys. Rev. C 94, 014609 (2016). https://doi.org/10.1103/PhysRevC.94.014609
- 50. A. Rodriguez Manso, A.B. McIntosh, A. Jedele et al., Detailed characterization of neutron-proton equilibration in dynamically deformed nuclear systems. Phys. Rev. C 95, 044604 (2017)
- 51. H.S. Wang, J. Xu, B.A. Li et al., Reexamining the isospinrelaxation time in intermediate-energy heavy-ion collisions. Phys. Rev. C 98, 054608 (2018). https://doi.org/10.1103/PhysR evC.98.054608
- 52. R. Bougault, E. Bonnet, B. Borderie et al., Light charged clusters emitted in 32 MeV/nucleon ^{136,124}Xe+^{124,112}Sn reactions: Chemical equilibrium and production of ³He and ⁶He. Phys. Rev. C 97, 024612 (2018). https://doi.org/10.1103/PhysRevC. 97.024612
- 53. L.W. May, A. Wakhle, A.B. McIntosh et al., Neutron-proton equilibration in 35 MeV/ u collisions of 64,70 Zn + 64,70 Zn and 64 Zn, ⁶⁴ Ni + ⁶⁴ Zn, ⁶⁴ Ni quantified using triplicate probes. Phys. Rev. C 98, 044602 (2018). https://doi.org/10.1103/PhysRevC.98.
- 54. Q. Fable, A. Chbihi, J.D. Frankland et al., [INDRA], Experimental study of isospin transport with 40,48Ca+40,48Ca reactions at 35 MeV/nucleon. Phys. Rev. C 107, 014604 (2023). https://doi.org/ 10.1103/PhysRevC.107.014604



- 55. E. De Filippo, A. Pagano, Experimental effects on dynamics and thermodynamics in nuclear reactions on the symmetry energy as seen by the CHIMERA 4π detector. Eur. Phys. J. A **50**, 32 (2014). https://doi.org/10.1140/epja/i2014-14032-y
- V. Baran, M. Colonna, M. Di Toro et al., Isospin effects in nuclear fragmentation. Nucl. Phys. A 703, 603–632 (2002). https://doi.org/10.1016/S0375-9474(01)01671-2
- V. Baran, M. Colonna, M. Di Toro, Neck fragmentation reaction mechanism. Nucl. Phys. A 730, 329–354 (2004). https://doi.org/ 10.1016/j.nuclphysa.2003.10.022
- V. Baran, M. Colonna, M. Di Toro et al., Isospin transport at Fermi energies. Phys. Rev. C 72, 064620 (2005). https://doi.org/ 10.1103/PhysRevC.72.064620
- M. Colonna, V. Baran, M. Di Tor, Theoretical predictions of experimental observables sensitive to the symmetry energy. Eur. Phys. J. A 50, 30 (2014). https://doi.org/10.1140/epja/ i2014-14030-1
- M. Colonna, Collision dynamics at medium and relativistic energies. Prog. Part. Nucl. Phys. 113, 103775 (2020). https://doi.org/10.1016/j.ppnp.2020.103775Colonna:2020euy
- L.W. Chen, C.M. Ko, B.A. Li, Light cluster production in intermediate-energy heavy ion collisions induced by neutron rich nuclei. Nucl. Phys. A 729, 809–834 (2003). https://doi.org/10.1016/j.nuclphysa.2003.09.010
- Y. Wang, C. Guo, Q. Li et al., ³H/³He ratio as a probe of the nuclear symmetry energy at sub-saturation densities. Eur. Phys. J. A 51, 37 (2015). https://doi.org/10.1140/epja/i2015-15037-8
- T. Gaitanos, M. Colonna, M. Di et al., Stopping and isospin equilibration in heavy ion collisions. Phys. Lett. B 595, 209–215 (2004). https://doi.org/10.1016/j.physletb.2004.05.080
- 64. G.C. Yong, B.A. Li, L.W. Chen et al., Triton-He-3 relative and differential flows as probes of the nuclear symmetry energy at supra-saturation densities. Phys. Rev. C 80, 044608 (2009). https://doi.org/10.1103/PhysRevC.80.044608
- P. Chomaz, F. Gulminelli, Phase transition in an isospin dependent lattice gas model. Phys. Lett. B 447, 221–226 (1999). https://doi.org/10.1016/S0370-2693(99)00003-9
- S. Albergo, S. Costa, E. Costanzo et al., Temperature and freenucleon densities of nuclear matter exploding into light clusters in heavy-ion collisions. Nuovo Cim. A 89, 1–28 (1985). https:// doi.org/10.1007/BF02773614
- H.S. Xu, M.B. Tsang, T.X. Liu et al., Isospin fractionation in nuclear multifragmentation. Phys. Rev. Lett. 85, 716–719 (2000). https://doi.org/10.1103/PhysRevLett.85.716
- M.A. Famiano, T. Liu, W.G. Lynch et al., Neutron and proton transverse emission ratio measurements and the density dependence of the asymmetry term of the nuclear equation of state. Phys. Rev. Lett. 97, 052701 (2006). https://doi.org/10.1103/ PhysRevLett.97.052701
- S. Nagamiya, M.C. Lemaire, E. Moller, Production of pions and light fragments at large angles in high-energy nuclear collisions. Phys. Rev. C 24, 971–1009 (1981). https://doi.org/10.1103/ PhysRevC.24.971
- M. Veselsky, R.W. Ibbotson, R. Laforest et al., Isospin dependence of isobaric ratio Y(³H) / Y(³He) and its possible statistical interpretation. Phys. Lett. B 497, 1–7 (2001). https://doi.org/10.1016/S0370-2693(00)01318-6
- F. Rami, Y. Leifels, B. de Schauenburg et al., [FOPI], Isospin tracing: a Probe of nonequilibrium in central heavy ion collisions. Phys. Rev. Lett. 84, 1120–1123 (2000). https://doi.org/10.1103/PhysRevLett.84.1120
- Y.B. Gurov, L.Y. Korotkova, S.V. Lapushkin et al., Yields of triton and ³He produced by nuclei in reactions of stopped pion absorption. Bull. Russ. Acad. Sci. Phys. 78, 1112–1116 (2014). https://doi.org/10.3103/S1062873814110100

- 73. G. Poggi, G. Pasquali, M. Bini et al., Evidence for collective expansion in light-particle emission following Au+Au collisions at 100, 150 and 250 A MeV. Nucl. Phys. A **586**, 755–776 (1995). https://doi.org/10.1016/0375-9474(95)00042-Y
- 74. R. Bougault, P. Eudes, D. Gourio et al., A possible scenario for the time dependence of the multifragmentation process in Xe+ Sn collisions: an explanation of the ³He puzzle. (an explanation of the ³He puzzle). International Winter Meeting on Nuclear Physics 35, Feb 1997, Bormio, Italy. pp. 251–275. in2p3-00023111
- T.X. Liu, W.G. Lynch, R.H. Showalter et al., Isospin observables from fragment energy spectra. Phys. Rev. C 86, 024605 (2012). https://doi.org/10.1103/PhysRevC.86.024605
- 76. M.A. Lisa, S. Albergo, F. Bieser et al., [EOS], Radial flow in Au + Au collisions at E = (0.25-1.15)-A GeV. Phys. Rev. Lett. 75, 2662–2665 (1995). https://doi.org/10.1103/PhysRevLett.75. 2662
- A. Bonasera, M. Bruno, C. Dorso et al., Critical phenomena in nuclear fragmentation. Rivista del Nuovo Cimento 23, 1–101 (2000). https://doi.org/10.1007/BF03548882
- W. Neubert, A.S. Botvina, What is the physics behind the ³He ⁴He anomaly? Eur. Phys. J. A 7, 101–106 (2000). https://doi.org/10.1007/s100500050016
- D.V. Shetty, A. Keksis, E. Martin et al., Intermediate mass fragments and isospin dependence in ¹²⁴Sn, ¹²⁴Xe + ¹²⁴Sn, ¹¹²Sn reactions at 28-MeV/nucleon. Phys. Rev. C 68, 054605 (2003). https://doi.org/10.1103/PhysRevC.68.054605
- 80. S. Piantelli, G. Casini, A. Ono et al., Isospin transport phenomena for the systems ⁸⁰Kr+^{40,48}Ca at 35 MeV/nucleon. Phys. Rev. C 103, 014603 (2021). https://doi.org/10.1103/PhysRevC.103. 014603
- W. Reisdorf, [FOPI] et al., Systematics of central heavy ion collisions in the 1A GeV regime. Nucl. Phys. A 848, 366–427 (2010). https://doi.org/10.1016/j.nuclphysa.2010.09.008
- F. Guan, X. Diao, Y. Wang et al., A compact spectrometer for heavy Ion experiments in the fermi energy regime. Nucl. Instrum. Meth. A 1011, 165592 (2021). https://doi.org/10.1016/j.nima. 2021.165502
- Y.J. Wang, F.H. Guan, X.Y. Diao et al., CSHINE for studies of HBT correlation in heavy Ion reactions. Nucl. Sci. Tech. 32, 4 (2021). https://doi.org/10.1007/s41365-020-00842-2
- Z. Sun, W.L. Zhan, Z.Y. Guo et al., RIBLL, the radioactive ion beam line in Lanzhou. Nucl. Instrum. Meth. A 503, 496–503 (2003). https://doi.org/10.1016/S0168-9002(03)01005-2
- 85. J.W. Xia, W.L. Zhan, B.W. Wei et al., The heavy ion cooler-stor-age-ring project (HIRFL-CSR) at Lanzhou. Nucl. Instrum. Meth. A 488, 11–25 (2002). https://doi.org/10.1016/S0168-9002(02) 00475-8
- 86. F. Guan, Y. Wang, X. Diao et al., Track recognition for the ΔE-E telescopes with silicon strip detectors. Nucl. Instrum. Meth. A 1029, 166461 (2022). https://doi.org/10.1016/j.nima. 2022.166461
- X.Y. Diao, F.H. Guan, Y.J. Wang et al., Reconstruction of fission events in heavy ion reactions with the compact spectrometer for heavy ion experiment. Nucl. Sci. Tech. 33, 40 (2022). https://doi. org/10.1007/s41365-022-01024-y
- X. Wei, F. Guan, H. Yang et al., Development of parallel plate avalanche counter for heavy ion collision in radioactive ion beam. Nucl. Eng. Tech. 52, 575–580 (2020). https://doi.org/10.1016/j. net.2019.08.020
- D. Guo, Y. Qin, S. Xiao et al., An FPGA-based trigger system for CSHINE. Nucl. Sci. Tech. 33, 162 (2022). https://doi.org/10. 1007/s41365-022-01149-0
- Y. Zhang, N. Wang, Q.F. Li et al., Progress of quantum molecular dynamics model and its applications in heavy ion collisions.



- Front. Phys. (Beijing) 15, 54301 (2020). https://doi.org/10.1007/ s11467-020-0961-9
- 91. R.J. Charity, M.A. McMahan, G.J. Wozniak et al., Systematics of complex fragment emission in niobium-induced reactions. Nucl. Phys. A 483, 371-405 (1988). https://doi.org/10.1016/ 0375-9474(88)90542-8
- 92. R.J. Charity, L.G. Sobotka, J. Cibor et al., Emission of unstable clusters from hot Yb compound nuclei. Phys. Rev. C 63, 024611 (2001). https://doi.org/10.1103/PhysRevC.63.024611
- 93. J. Aichelin, C. Hartnack, A. Bohne et al., QMD versus BUU/ VUU: same results from different theories. Phys. Lett. B 224, 34-39 (1989). https://doi.org/10.1016/0370-2693(89)91045-9
- 94. J. Aichelin, 'Quantum' molecular dynamics: a dynamical microscopic n body approach to investigate fragment formation and the nuclear equation of state in heavy ion collisions. Phys. Rept. 202, 233–360 (1991). https://doi.org/10.1016/0370-1573(91)90094-3
- 95. R.S. Wang, L. Ou, Z.G. Xiao, Production of high-energy neutron beam from deuteron breakup. Nucl. Sci. Tech. 33, 92 (2022). https://doi.org/10.1007/s41365-022-01075-1
- 96. L. Ou, Z.G. Xiao, Orientation dichroism effect of proton scattering on deformed nuclei. Chin. Phys. C 44, 114103 (2020). https:// doi.org/10.1088/1674-1137/abadf1
- 97. X. Liang, L. Ou, Z. Xiao, New probe to study the symmetry energy at low nuclear density with the deuteron breakup reaction. Phys. Rev. C 101, 024603 (2020). https://doi.org/10.1103/PhysR evC.101.024603
- 98. L.W. Chen, C.M. Ko, B.A. Li et al., Density slope of the nuclear symmetry energy from the neutron skin thickness of heavy nuclei. Phys. Rev. C 82, 024321 (2010). https://doi.org/10.1103/ PhysRevC.82.024321
- 99. Y. Zhang, Z. Li, C. Zhou et al., Effect of isospin dependent cluster recognition on the observables in heavy ion collisions. Phys. Rev. C 85, 051602 (2012). https://doi.org/10.1103/PhysRevC.85. 051602
- 100. J. Zheng, E. Wu, C. Zhang et al., Measurement of fission time scale and excitation energy at scission for 25 MeV/u ⁴⁰Ar+²⁰⁹Bi fission reaction. Chinese Phys. C 23, 946-953 (1999)
- 101. H.H. Gutbrod, A. Sandoval, P.J. Johansen et al., Final state interactions in the production of hydrogen and helium isotopes by relativistic heavy ions on uranium. Phys. Rev. Lett. 37, 667-670 (1976). https://doi.org/10.1103/PhysRevLett.37.667
- 102. W. Reisdorf, D. Best, A. Gobbi et al. [FOPI], Central collisions of Au on Au at 150, 250 and 400 MeV/nucleon. Nucl. Phys. A **612**, 493-556 (1997). https://doi.org/10.1016/S0375-9474(96) 00388-0
- 103. H. Xi, M.J. Huang, W.G. Lynch et al., Examining the cooling of hot nuclei. Phys. Rev. C 57, R462-R465 (1998). https://doi.org/ 10.1103/PhysRevC.57.R462
- 104. A.R. Raduta, E. Bonnet, B. Borderie et al., Break-up stage restoration in multifragmentation reactions. Eur. Phys. J. A 32, 175-182 (2007). https://doi.org/10.1140/epja/i2006-10381-4
- 105. L.G. Sobotka, Simulations of collisions between nuclei at intermediate energy using the Boltzmann-Uehling-Uhlenbeck equation with neutron skin producing potentials. Phys. Rev. C 50, R1272-R1275 (1994). https://doi.org/10.1103/PhysRevC.50.
- 106. R. Lionti, V. Baran, M. Colonna et al., Isospin dynamics in fragmentation reactions at Fermi energies. Phys. Lett. B 625, 33 (2005). https://doi.org/10.1016/j.physletb.2005.08.044
- 107. V. Baran, M. Colonna, V. Greco et al., Reaction dynamics with exotic beams. Phys. Rept. 410, 335-466 (2005). https://doi.org/ 10.1016/j.physrep.2004.12.004

- 108. D.D.S. Coupland, W.G. Lynch, M.B. Tsang et al., Influence of transport variables on isospin transport ratios. Phys. Rev. C 84, 054603 (2011). https://doi.org/10.1103/PhysRevC.84.054603
- 109. V. Baran, M. Colonna, M. Di Toro et al., From multifragmentation to neck fragmentation: mass, isospin, and velocity correlations. Phys. Rev. C 85, 054611 (2012), https://doi.org/10.1103/ PhysRevC.85.054611
- 110. L.G. Sobotka, R.J. Charity, D.K. Agnihotri et al., Neutron-proton asymmetry of the midvelocity material in an intermediate-energy heavy ion collision. Phys. Rev. C 62, 031603 (2000). https://doi. org/10.1103/PhysRevC.62.031603
- 111. S. Piantelli, P.R. Maurenzig, A. Olmi et al., Distinctive features of Coulomb-related emissions in peripheral heavy ion collisions at Fermi energies. Phys. Rev. C 76, 061601 (2007). https://doi. org/10.1103/PhysRevC.76.061601
- 112. E. Vient et al. [INDRA], New "3D calorimetry" of hot nuclei. Phys. Rev. C 98, 044611 (2018). https://doi.org/10.1103/PhysR evC.98.044611
- 113. E. Plagnol, J. Lukasik, G. Auger et al., Onset of midvelocity emissions in symmetric heavy ion reactions. Phys. Rev. C 61, 014606 (2000). https://doi.org/10.1103/PhysRevC.61.014606
- 114. S. Piantelli, L. Bidini, G. Poggi et al., Intermediate mass fragment emission pattern in peripheral heavy-ion collisions at Fermi energies. Phys. Rev. Lett. 88, 052701 (2002). https://doi.org/10. 1103/PhysRevLett.88.052701
- 115. D. Theriault, J. Gauthier, F. Grenier et al., Neutron to proton ratios of quasiprojectile and midrapidity emission in the ⁶⁴Zn + ⁶⁴Zn reaction at 45-MeV/nucleon. Phys. Rev. C **74**, 051602 (2006). https://doi.org/10.1103/PhysRevC.74.051602
- 116. R. Planeta et al. [ISOSPIN], Centrality dependence of isospin effect signatures in ¹²⁴Sn + ⁶⁴Ni and ¹¹²Sn + ⁵⁸Ni reactions. Phys. Rev. C 77, 014610 (2008). https://doi.org/10.1103/PhysRevC.77. 014610
- 117. Z. Kohley, L.W. May, S. Wuenschel et al., Transverse collective flow and midrapidity emission of isotopically identified light charged particles. Phys. Rev. C 83, 044601 (2011). https://doi. org/10.1103/PhysRevC.83.044601
- 118. R. Ogul, A.S. Botvina, M. Bleicher et al., Isospin compositions of correlated sources in the Fermi energy domain. Phys. Rev. C 107, 054606 (2023). https://doi.org/10.1103/PhysRevC.107.054606
- 119. Y. Qin, Q. Niu, D. Guo et al., Probing high-momentum component in nucleon momentum distribution by neutron-proton bremsstrahlung γ -rays in heavy ion reactions. Phys. Lett. B **850**, 138514 (2024). https://doi.org/10.1016/j.physletb.2024.138514
- 120. R. Wang, Y.G. Ma, L.W. Chen et al., Kinetic approach of lightnuclei production in intermediate-energy heavy-ion collisions. Phys. Rev. C 108, L031601 (2023). https://doi.org/10.1103/ PhysRevC.108.L031601
- 121. K. Pomorski, B. Nerlo-Pomorska, A. Surowiec et al., Light particle emission from the fissioning nuclei Ba-126, Pt-188 and 110-266, 110-272, 110-278: theoretical predictions and experimental results. Nucl. Phys. A 679, 25-53 (2000). https://doi.org/ 10.1016/S0375-9474(00)00327-4

Springer Nature or its licensor (e.g. a society or other partner) holds exclusive rights to this article under a publishing agreement with the author(s) or other rightsholder(s); author self-archiving of the accepted manuscript version of this article is solely governed by the terms of such publishing agreement and applicable law.



155 Page 12 of 12 Y.-J. Wang et al.

Authors and Affiliations

Yi-Jie Wang¹® · Sheng Xiao¹ · Meng-Ting Wan²,³ · Xin-Yue Diao¹® · Yu-Hao Qin¹® · Zhi Qin¹® · Dong Guo¹ · Da-Wei Si¹ · Bo-Yuan Zhang¹ · Bai-Ting Tian¹ · Jun-Huai Xu¹ · Fen-Hai Guan¹® · Qiang-Hua Wu¹ · Xiang-Lun Wei⁴ · He-Run Yang⁴ · Peng Ma⁴ · Rong-Jiang Hu⁴ · Li-Min Duan⁴® · Fang-Fang Duan⁴ · Jun-Bing Ma⁴ · Shi-Wei Xu⁴ · Qiang Hu⁴ · Zhen Bai⁴ · Yan-Yun Yang⁴® · Jian-Song Wang⁴,⁵® · Wen-Bo Liu⁶ · Wan-Qing Su⁶® · Xiao-Bao Wei⁶® · Chun-Wang Ma⁶® · Xin-Xiang Li²,⁵ · Hong-Wei Wang⁵,⁵® · Ying-Xun Zhang¹⁰ · Michał Warda¹³ · Arthur Dobrowolski¹³ · Bożena Nerlo-Pomorska¹³ · Krzysztof Pomorski¹¹ · Li Ou²,³® · Zhi-Gang Xiao¹,¹²®

- Yi-Jie Wang yj-wang15@tsinghua.org.cn
- ☑ Li Ou liou@gxnu.edu.cn
- ⊠ Zhi-Gang Xiao xiaozg@tsinghua.edu.cn
- Department of Physics, Tsinghua University, Beijing 100084, China
- College of Physics and Technology, Guangxi Normal University, Guilin 541004, China
- Guangxi Key Laboratory of Nuclear Physics and Technology, Guangxi Normal University, Guilin 541004, China
- Institute of Modern Physics, Chinese Academy of Sciences, Lanzhou 730000, China
- School of Science, Huzhou University, Huzhou 313000, China

- Institute of Particle and Nuclear Physics, Henan Normal University, Xinxiang 453007, China
- School of Nuclear Science and Technology, University of South China, Hengyang 421001, China
- Shanghai Institute of Applied Physics, Chinese Academy of Science, Shanghai 201800, China
- Shanghai Advanced Research Institute, Chinese Academy of Science, Shanghai 201210, China
- China Institute of Atomic Energy, Beijing 102413, China
- National Centre for Nuclear Research, 02-093 Warsaw, Poland
- Collaborative Innovation Center of Quantum Matter, Tsinghua University, Beijing 100084, China
- ¹³ Institute of Physics, Maria Curie Skłodowska University, 20-031 Lublin, Poland

